

Original Article

Pathology of non-thermal irreversible electroporation (N-TIRE)-induced ablation of the canine brain

John H. Rossmeisl Jr.^{1,*}, Paulo A. Garcia², John L. Roberston³, Thomas L. Ellis⁴, Rafael V. Davalos²

Departments of¹Small Animal Clinical Sciences, and³Biomedical Sciences and Pathobiology, Virginia-Maryland Regional College of Veterinary Medicine, ²Bioelectromechanical Systems Laboratory, School of Biomedical Engineering and Sciences, Virginia-Tech Wake Forest University School of Biomechanical Engineering, Virginia Tech, Blacksburg, VA 24061, USA
⁴Wake Forest University School of Medicine, Winston-Salem, NC 27157, USA

This study describes the neuropathologic features of normal canine brain ablated with non-thermal irreversible electroporation (N-TIRE). The parietal cerebral cortices of four dogs were treated with N-TIRE using a dose-escalation protocol with an additional dog receiving sham treatment. Animals were allowed to recover following N-TIRE ablation and the effects of treatment were monitored with clinical and magnetic resonance imaging examinations. Brains were subjected to histopathologic and ultrastructural assessment along with Bcl-2, caspase-3, and caspase-9 immunohistochemical staining following sacrifice 72 h post-treatment. Adverse clinical effects of N-TIRE were only observed in the dog treated at the upper energy tier. MRI and neuropathologic examinations indicated that N-TIRE ablation resulted in focal regions of severe cytoarchitectural and blood-brain-barrier disruption. Lesion size correlated to the intensity of the applied electrical field. N-TIRE-induced lesions were characterized by parenchymal necrosis and hemorrhage; however, large blood vessels were preserved. A transition zone containing parenchymal edema, perivascular inflammatory cuffs, and reactive gliosis was interspersed between the necrotic focus and normal neuropil. Apoptotic labeling indices were not different between the N-TIRE-treated and control brains. This study identified N-TIRE pulse parameters that can be used to safely create circumscribed foci of brain necrosis while selectively preserving major vascular structures.

Keywords: central nervous system, dog, irreversible electroporation, neuropathology

Introduction

Electroporation is a technique that involves the delivery

of low-energy electrical pulses to tissues, resulting in cell permeabilization, either reversibly or irreversibly, through the formation of nanoscale porous channels in the cellular membranes [23]. The precise mechanism by which electrical pulses cause membrane permeabilization is unknown. It has been postulated that the electrical potential induced across cell membranes disrupts the lipid bilayer, resulting in localized alteration of the membrane shape and creation of aqueous pores through which molecules can pass [4,23]. Application of an electrical field at strengths above tissue-specific critical threshold values causes cell death in the treated volume via irreversible electroporation (IRE) [6]. It has been reported that certain electric field parameters can induce IRE without causing thermal damage to treated tissue [6,21], a process referred to as non-thermal IRE (N-TIRE).

IRE and N-TIRE have only recently been used for *in vivo* ablation of soft tissue tumors [1,19]. The thermal sparing effect of N-TIRE offers distinct advantages compared to thermally mediated tissue destruction methods such as cryoablation [22], laser interstitial thermotherapy [2], radiofrequency lesioning [5], and high-frequency ultrasound [11]. Studies of focal N-TIRE using porcine liver and canine prostate have shown that therapeutic protocols can be designed which spare sensitive tissues such as the major vasculature, ductal frameworks, or nerve tissues within the treated parenchymal volumes [18,20]. In addition, there is a region of increased membrane permeability (reversibly electroporated cells) with N-TIRE that is formed outside the zone of irreversible tissue ablation [6,16]. The temporary increase in membrane permeability of tissues within this reversibly electroporated penumbra can be used to promote local

*Corresponding author: Tel: +1-540-231-4621; Fax: +1-540-231-1676; E-mail: jrossmei@vt.edu

delivery of cytotoxic compounds for targeted death of neoplastic cells [7,16]. These properties prompted us to investigate the use of N-TIRE as a focal ablative technique in the brain with the intent of exploiting its advantages for treating malignant glioma. We previously reported that N-TIRE can be used to predictably, safely, and focally ablate areas of normal and neoplastic canine brain tissue using electrical charges in the lower spectrum of those delivered to the human brain during electroconvulsive therapy [9,12].

Previous studies have provided limited descriptions of N-TIRE-induced tissue injury in the liver, prostate, brain, and vasculature [9,14,15,18]. In these investigations, both apoptotic and necrotic cell death in tissues following acute to subacute N-TIRE ablation were observed [14,15,18]. Since electroporation-induced cell death occurs through currently unknown pathways, the evaluation of N-TIRE-treated tissues should provide insight into the underlying mechanisms of injury. Here we describe in detail the acute pathological features of *in vivo* experimental canine brain ablation with N-TIRE.

Materials and Methods

All study procedures were approved by the Virginia Tech Institutional Animal Care and Use Committee (08-218-CVM). Experimental dogs were cared for according to the National Research Council guidelines [17] for laboratory animals, and the experiments were performed in a Good Laboratory Practices-compliant facility (Clinical Research Laboratory, Virginia-Maryland Regional College of Veterinary Medicine, VA, USA).

In vivo N-TIRE canine brain ablation procedure

Five clinically normal, neurologically intact, 2-year-old, purpose-bred Beagle crossbred dogs (Covance, USA) weighing 11 ~ 14 kg were used for this study. The N-TIRE ablation procedure we performed has been described elsewhere [9]. Briefly, general anesthesia was induced with intravenous (IV) diazepam (1 mg/kg; Abbott Laboratories, USA), propofol (4 ~ 6 mg/kg; Abbott Laboratories), and fentanyl (10 µg/kg/hr; Abbott

Laboratories). Magnetic resonance imaging (MRI) examination of the brain was then performed with a low-field magnet (0.2 T Vet-MRI; Esaote S.p.A., Italy) using standard T1-weighted (T1W), T2-weighted (T2W), fluid attenuated inversion recovery (FLAIR), and T1W-post gadolinium sequences in three planes. A routine right lateral rostral approach to the canine skull was performed. Right parietotemporal craniectomy defects were created with a high-speed pneumatic drill (Hall Surgairtome Two; ConMed, USA), and regional dural resections were performed along the limits of the craniectomy. N-TIRE lesions were created in the right parietal lobe of the cerebrum in four dogs (Table 1) using a NanoKnife pulse generator and electrodes (AngioDynamics, USA). An additional dog underwent a sham control procedure (Table 1). The lesions were created by administering nine sets of ten electrical pulses at a repetition rate of 4 Hz. The pulses were each 50 µseconds in duration and configured with alternating polarity between each set to minimize charge build-up on the electrode surface. The sets were delivered every 3.5 seconds. The strength of the electric field applied in this configuration was calculated based on the voltage-to-distance ratio between the energized and grounded electrodes (Table 1) [9]. For the sham procedure, the electrodes were placed in the cerebral cortex for 2 min without delivering electrical pulses. The left hemisphere served as an internal (untreated) control for each dog.

Additional MRI data were obtained 1 h after N-TIRE. The dogs were then allowed to recover from anesthesia and received subcutaneous buprenorphine (0.05 mg/kg; Abbott Laboratories) every 8 h for 48 h. During the recovery period, physical and neurological examinations were performed every 6 h for 72 h, and the dogs were then humanely sacrificed by intravenous barbiturate overdose (35 mg/kg, Beuthanasia-D; Abbott Laboratories). Immediately following euthanasia, the dogs were infused with physiologic saline for 15 min to maintain a hydrostatic pressure of 90 mm Hg.

Gross and microscopic examination of brain tissue

Formalin-fixed brains were cut into 5-mm sections (5

Table 1. N-TIRE treatment parameters

Dog	Electrode configuration	Exposure area length (mm)	Interelectrode gap (mm)	Voltage (V)	Voltage-to-distance ratio	Pulses/pulse duration (µsec)	Charge delivered (mC)
1	Monopolar	5	5	Sham	Sham	Sham	Sham
2	Monopolar	5	5	500	1,000	90/50	1.47
3	Monopolar	5	5	1,000	2,000	90/50	9.89
4	Bipolar	Standard	7	1,600	2,000	90/50	13.08
5	Monopolar	5	10	2,000	2,000	90/50	22.23

mm Porcine Matrix Slicer; Zivic Instruments, USA) in the transverse plane from the olfactory bulb through the cervicomedullary junction and embedded in paraffin. The paraffin-embedded sections were then cut into 5- μ m sections, mounted on positively charged slides (Fisher Scientific, USA) and stained with hematoxylin and eosin (H&E; Fisher Scientific), luxol fast blue and Periodic Acid Schiff (LFB-PAS; Hitobiotech, USA), modified trichrome (TRIC; Fisher Scientific), Bielschowsky silver (BS; Abcam, USA), and glial fibrillary acidic protein (GFAP; Millipore, USA) according to standard procedures [10].

Electron microscopy

Brain tissues were fixed in buffered 2.5% glutaraldehyde (Fisher Scientific), post-fixed in buffered 1% osmium tetroxide (Fisher Scientific), dehydrated in graded series of 35~100% ethanol and propylene oxide (Sigma Aldrich, USA), trimmed, and then embedded in epoxy. One- μ m sections were stained with 1% toluidine blue (Fisher Scientific) and 2% borate in distilled water, air dried, and examined by light microscopy (Eclipse; Nikon, Japan) to select representative fields for electron microscopy. The tissue samples were then cut into 50-nm sections (EM UC7; Lecia Microsystems, Germany), stained with uranyl acetate (Fisher Scientific) for 2 hours and lead citrate (Fisher Scientific) for 5 minutes, and examined using a transmission electron microscope (EMC-10 CA; Carl Zeiss AG, Germany).

Bcl-2, caspase-3, caspase-9, and factor VIII-related antigen immunohistochemistry (IHC)

Formalin-fixed, paraffin-embedded, transversely oriented, brain tissue samples were cut into 5- μ m sections for IHC studies. The sections were stained using an automated system (Dako Autostainer; Dako, USA). Antigen retrieval was performed in 10 mM citrate buffer (pH 6.0) with two 5-min cycles of microwaving at 600 W and 2.5 GHz (Bcl-2) or by incubating for 30 min at 37°C in a proteinase K solution (CD31; IHC-Tek, USA). Antigen retrieval for caspase-3 and caspase-9 was performed with antigen retrieval citrate buffer (citrate pH 6.0; caspase-3, EDTA pH 9.0; caspase-9, Dako 3-in-1; Dako) in a DAKO PT Link (Dako) by boiling for 10 (caspase-3) or 15 (caspase-9) min. The sections were washed in neutral PBS for 5 min following antigen retrieval. Endogenous peroxidase activity was quenched by exposing the sections to 0.3% hydrogen peroxide in methanol for 30 min at room temperature. After blocking with 10% normal goat serum (Genway Biotech, USA) for 30 min at 37°C, the sections were incubated with rabbit polyclonal antibodies against Bcl-2 (1 : 100; Abcam) caspase-3 (1 : 60; Abcam), caspase-9 (1 : 100; Abcam), and CD31/PECAM-1 (1 : 200, Bioss, USA) in 0.01 M PBS

containing 1% normal goat serum and 0.3% Triton X-100 for 30 min at 20°C. The sections were then rinsed with Tris buffered saline and incubated for 40 min (CD31) or 1 h (Bcl-2, caspase-3, and caspase-9) at 37°C with anti-mouse or biotinylated anti-rabbit IgG (1 : 200, ABC kit; Vector Laboratories, USA) in 0.01 M PBS containing 1% normal goat serum and 0.3% Triton X-100 [3]. Subsequently, the sections were rinsed with Tris buffered saline and incubated with an avidin-biotin-horseradish peroxidase complex (1 : 200, ABC kit; Vector Laboratories) for 1 h at 37°C. The slides were chromogenically developed with 3,3'-diaminobenzidine tetrahydrochloride (Dako Cytomation, USA) for 5 min at room temperature and then counterstained with Fast Red (Ventana Medical Systems, USA). Positive controls for IHC included canine tonsil (caspase-3), normal canine brain tissue (CD31), canine mammary adenocarcinoma (caspase-9), and murine hippocampus (Bcl-2). Positive control tissues were obtained from the Necropsy and Veterinary Pathology Service of the Virginia-Maryland Regional College of Veterinary Medicine, VA, USA. Negative control sections received identical treatment except that they were not exposed to the primary antibodies.

Computer-aided analysis of IHC apoptotic indices

Apoptotic indices were determined to quantitate the degree of apoptosis in the histological sections stained for Bcl-2, caspase-3, and caspase-9. This was done using an equation to calculate the percentage of positively labeled cells per the total number of cells in a section:

$$x \text{ Labeling Index (xLI)} = \frac{\text{Number of } x \text{ immunoreactive cells} \times 100}{\text{Total number of nuclei}}$$

Images of the microscopic fields of interest in the treated and homologous contralateral control cerebral cortices were captured with a charge-coupled device digital camera (DS-Fi2; Nikon). In addition, the right parietal cerebral cortices from three normal aged-matched, purpose-bred Beagle dogs (Covance) that were euthanized for reasons unrelated to this study were examined as untreated controls. The digitized images were optically segmented using density and size thresholding techniques in order to discriminate negative from positive (Image J version 1.46r, National Institute of Health, USA). This segmentation process allowed the generation of binary images from which the number of positively stained objects, as indicated by a chromogen intensity greater or equal to that of positive control tissue, in each region of interest could be determined. To calculate the labeling indices for each immunohistochemical stain, five random 200 \times fields were selected from each slide and at least 1,000 total cells were counted.

Statistical analysis

Differences in apoptosis LI values between N-TIRE-treated and control brain sections for each staining procedure (Bcl-2, caspase-3, and caspase-9) were compared using an unpaired Student's *t*-test (SAS version 9.0; SAS Institute, USA). The *p* values < 0.05 were considered statistically significant.

Results

N-TIRE procedure

Dogs 1~4 recovered from the sham or N-TIRE procedures without complications. Results of the post-operative neurological examinations were normal within 12 h of surgery. Dog 5 (Table 1) developed signs consistent with transtentorial brain herniation (unilateral unresponsive mydriasis and decerebrate rigidity) ipsilateral to the area of N-TIRE treatment 14 h after the procedure. The animal was euthanized.

Brain MRI examinations

No abnormalities were detected by pre-treatment MRI in any dog (Figs. 1A and B). N-TIRE resulted in clearly marginalized, elliptical to ovoid defects of various size in the parietal lobe. The lesions were T1-iso- to hypointense (Figs. 1C and D), and predominantly T2 (Figs. 1E and F) and FLAIR hyperintense with central and peripheral regions of hypointensity. Peripheral contrast enhancement was observed following gadolinium administration (Figs. 1G and H).

Gross brain examination

Focal areas of hemorrhage and malacia in the right parietal region clearly defined the areas ablated by N-TIRE (Figs. 1I~L). There was excellent morphologic correlation between the MRI findings and pathologic features of the N-TIRE lesions (Figs. 1I~P). Data obtained from the gross brain sections indicated that the volumes of N-TIRE-affected tissue correlated positively with the applied electrical charges (Table 1, Fig. 1). In addition to the N-TIRE-induced lesion, right unilateral transtentorial herniation (Fig. 2A), marked edema of the white matter in the right cerebral hemisphere, and infarction of the right caudate nuclear area secondary to thrombosis of a penetrating artery were observed in Dog 5 (Fig. 2B). No lesions were found in the contralateral internal control hemispheres. In the sham-operated dog (Dog 1), gross examination revealed two punctate, 1-mm superficial cortical depressions consistent with the insertion points of the electrodes.

Light microscopic and ultrastructural examination

No significant lesions were noted during light microscopy evaluation of the control brain tissues (Fig. 3A). In brain sections from the sham-operated control dog, injury was limited to physical disruption of the neuropil in the electrode trajectory without any collateral damage

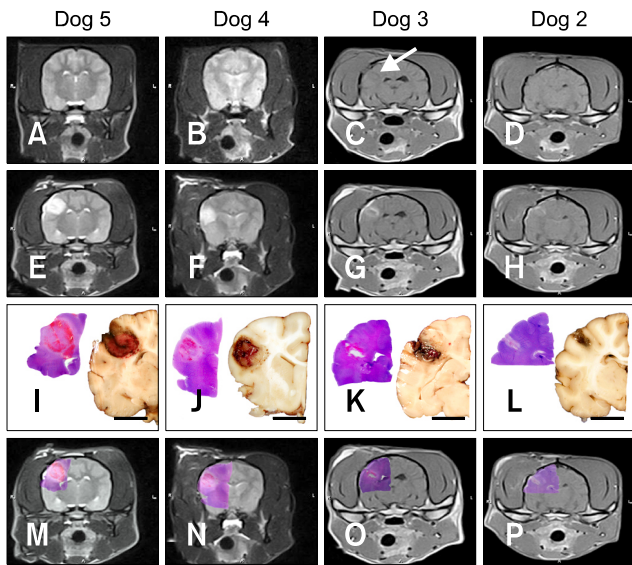


Fig. 1. Macroscopic morphology of non-thermal irreversible electroporation (N-TIRE) ablation in the right parietal lobe of the canine brain (Dogs 2~5). The caudal aspect of the lesion area in Dogs 2 and 3 is shown along with the rostral lesion area in Dogs 4 and 5. The right side of the brain is on the left side of the images in all panels. (A and B) Normal, pre-treatment T2W MR images. (C and D) Post-treatment T1W MR images showing a T1 iso- to hypointense lesion (white arrow). (E and F) Post-treatment T2W MR images containing focal, ovoid heterogeneously hyperintense lesions. (G and H) Post-treatment, post-contrast T1W MR images demonstrating peripheral contrast enhancement of the ablated regions. (I~L) Subgross (H&E) and gross pathologic features of brain sections corresponding to anatomic levels presented in the MR images in panels E~H. N-TIRE ablative lesions are characterized by malacia and intraparenchymal hemorrhage, and are clearly demarcated from the surrounding normal brain tissues. (M~P) Composite images generated by superimposing H&E-stained brain sections on the corresponding MRI slice. Scale bars = 1 cm (I~L).

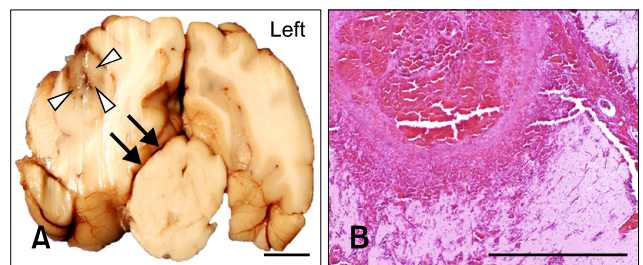


Fig. 2. Adverse effects associated with high-energy N-TIRE in Dog 5. (A) Right unilateral transtentorial herniation resulting in mesencephalic compression (black arrows) in the most caudal aspect of the N-TIRE-affected area (white arrowheads). (B) Cerebrocortical necrosis associated with marked vascular disruption and large artery thrombosis in the N-TIRE treatment region (H&E). Scale bars = 2.0 mm (B), 1cm (A).

(Fig. 3B). N-TIRE resulted in focal regions of severely disrupted gray (Fig. 3C) and white (Fig. 4) matter architecture that were sharply demarcated from the adjacent untreated brain tissue (Figs. 1 and 5A). Changes in the white matter consisted of diffuse edema (Figs. 4A and B), disrupted axonal projections, (Fig. 4B), and axonal spheroid formation (Fig. 4C).

N-TIRE gray matter lesions included a vacuolated amorphous coagulum and multifocal areas of intraparenchymal hemorrhage. The intraparenchymal hemorrhage was most pronounced in the gray matter in the electrode insertion trajectory (Fig. 3C), and the capillary beds in the peripheral junctional region between the treated and untreated areas of the brain (Fig. 5A). Remnant neurons within the treated regions were shrunken with hyper eosinophilic and angular cytoplasm as well as nuclear pyknosis or chromatolysis (Fig. 5B). Multifocal aggregates of inflammatory cells including neutrophils, lymphocytes, macrophages, and gitter cells were also found within the treated regions (Figs. 5B and C). Free glial nuclei in various states of degeneration (Fig. 5B) along with neuronal satellitosis and neuronophagia were also observed.

Within the treated regions of Dogs 2-4, blood vessels with

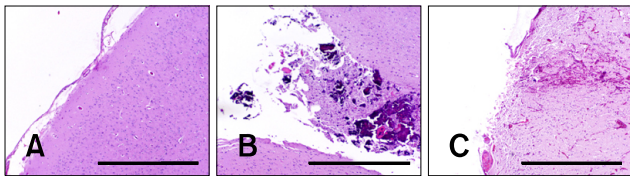


Fig. 3. Comparative effects of N-TIRE on the superficial parietal cerebral cortex. (A) Untreated, contralateral cortex of Dog 3. (B) Sham-operated cortex demonstrating physical disruption of the neuropil by the electrode in Dog 1. (C) Collateral cortical damage extending into the adjacent neuropil in N-TIRE-affected cortex of Dog 3. H&E, Scale bars = 2.0 mm (A ~C).

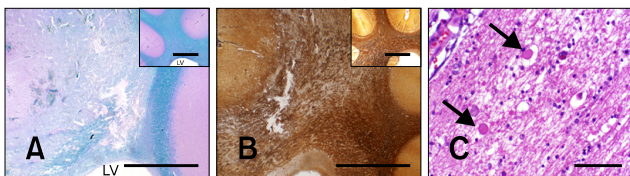


Fig. 4. Morphology of N-TIRE-induced lesions in the subcortical white matter of Dog 4. (A) Partial obliteration and vacuolization of the white matter in the corona radiata (luxol fast blue and Periodic Acid Schiff counterstain) with loss of the gray and white matter junctional distinction (inset, control). (B) Disruption of the axonal projections of the corona radiata (inset, control) of Dog 2 (Bielschowsky silver stain). (C) Vacuolar change in the white matter with axonal spheroids (arrows) in Dog 3 (H&E). LV: lateral ventricle. Scale bars = 200 μm (C), 5.0 mm (A, A inset, B and B inset).

luminal diameters exceeding 30 μm (Figs. 5C, 6A and B) appeared intact. In occasional endothelial cells within the unaffected vasculature, pyknosis with cytoplasmic eosinophilia and shrinkage were found. Separation of the tunica muscularis layers of the arterioles and diapedesis was also apparent in some sections. Collagenous scaffold morphology of large vessels within the N-TIRE-affected regions was preserved (Fig. 6C) and the endothelium of

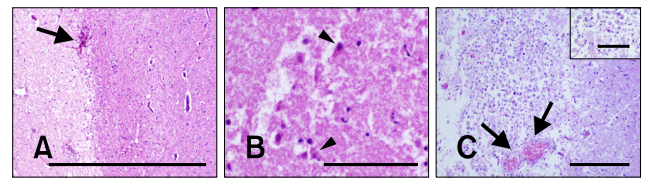


Fig. 5. Morphology of N-TIRE-induced lesions in the deep cortical gray matter. (A) N-TIRE ablated regions (left side of panel) were sharply demarcated from the adjacent normal brain (right side) identified by their pallor. A focus of intraparenchymal hemorrhage associated with a disrupted capillary bed was visible at the lesion periphery (arrow) in Dog 2. (B) Necrotic neurons (arrowheads) and degenerate free glial nuclei in the N-TIRE-associated lesion core in Dog 4. (C) Gitter cells and intact vessels (arrows) were present in the transition zone between the affected and normal brain tissue in Dog 3. H&E. Scale bars = 200 μm (B and C inset), 500 μm (C), 2.0 mm (A).

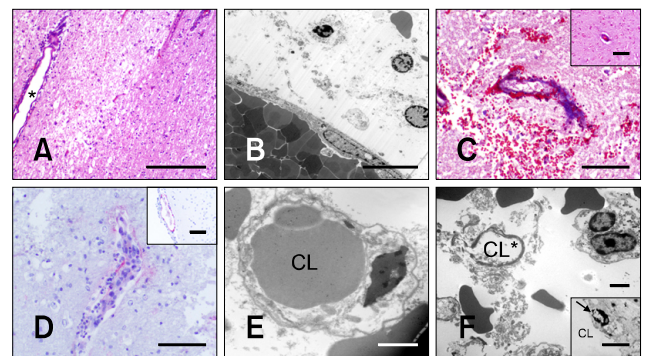


Fig. 6. Vascular sparing effects of N-TIRE. (A) A medium sized arteriole (*) at the periphery of the N-TIRE ablation region remained intact despite diffuse damage to the surrounding neuropil in Dog 3 (H&E). (B) Electron photomicrograph of a large vessel within the core N-TIRE ablation zone of Dog 4 in which the endothelial cytoarchitecture and intravascular erythrocytes were preserved. (C) Intact vascular collagenous scaffolds in N-TIRE-treated and control (inset) gray matter of Dog 4 (trichrome). (D) CD31-positive vascular endothelial immunoreactivity and perivascular inflammation in the core N-TIRE treatment region (inset, CD31 control). (E) Electron photomicrograph of an untreated control cerebral capillary. (F) Electron photomicrographs of capillaries within the core N-TIRE ablation zone with cytoplasmic and capillary luminal disruption (*), extravasted erythrocytes, and endothelial nuclear pyknosis (inset, arrow) in Dog 2. CL: capillary lumen. Scale bars = 2 μm (E, F and F inset), 10 μm (B), 200 μm (C, C inset, D and D inset), 500 μm (A).

intact vessels in the treated regions retained immunoreactivity to CD31 (Fig. 6D). Capillary endothelial cells demonstrated frequent pyknosis (Fig. 6F, inset) and were disrupted within regions of intraparenchymal hemorrhage (Fig. 6F). In contrast, there was complete disruption of tissue architecture and vasculature in the N-TIRE-induced lesions of Dog 5 (Fig. 2B).

Adjacent to the N-TIRE lesion interspersed between normal cerebrocortical tissue or underlying subcortical white matter was a transitional zone (TZ) characterized by vacuolization of the white and gray matter (Figs. 7A and B) and perivascular inflammatory cuffs (Fig. 7B). A rim of astrogliosis was also observed in the TZ. Severity of the glial reaction was proportional to the applied energy (Figs. 7B and C).

Immunohistochemical LI

No significant differences in Bcl-2, caspase-3, or caspase-9 LI values were noted between the N-TIRE-induced lesions, internal controls, or untreated

control samples (Fig. 8). Occasional Bcl-2 and caspase-3 immunoreactivity was found in vascular endothelial cells in all groups of dogs. Rarely, moderately intense immunostaining specific for Bcl-2 and caspase-9 was noted within random individual neurons in all layers of the cerebral cortex and hippocampus of all dogs.

Discussion

In the present study, we demonstrated that N-TIRE effectively ablated soft tissue of the brain and created zones of tissue destruction that were sharply demarcated from the surrounding normal areas. Despite extensive damage to most constitutive tissues within the core of N-TIRE-induced lesions, large blood vessels appeared structurally intact after treatment with specific voltages. The histomorphologic and IHC results indicated that cellular death is primarily mediated by necrosis in brain tissues examined 72 h following N-TIRE. We also provided guidelines for identifying the upper safety limit of applied energy when performing N-TIRE ablation of the brain. The energy delivered to Dog 5 resulted in IRE and thermal brain damage that resulted in vasogenic white matter edema, arterial thrombosis resulting in infarction, and subsequent clinically significant intracranial hypertension.

Our study illustrates several key advantages of N-TIRE over other current tissue ablation procedures. Margins of the N-TIRE ablation zones are demarcated from surrounding tissues with submillimeter resolution. This treatment localization phenomenon, coupled with the ability to mathematically model and predict the size of N-TIRE ablation zones [6,8,13,14], translates into the ability to create highly restricted regions of cell death. While the relative safety of more conventional, temperature-dependent ablation techniques has been demonstrated in the brain [5,22], the efficacy of these procedures is limited by a heat sink effect that results in the inconsistent ablation of tissues. As its name implies, N-TIRE does not result in any biologically significant thermal damage to the treated tissue [6,21], thus eliminating the heat sink effect. The general pathology of N-TIRE-induced tissue damage and vascular sparing in the brain is similar to that observed in the liver after N-TIRE [8,14].

The present study indicated that necrosis which was defined using classical morphologic criteria including loss of membrane integrity, organelle disruption, and induction of tissue inflammation is the predominant mechanism of cell death in brain tissue 72 h after N-TIRE ablation. No significant or specific immunoreactivity to Bcl-2, caspase-3, or caspase-9 was noted within the N-TIRE lesions. This findings suggest that apoptosis does not significantly contribute to cell death following N-TIRE.

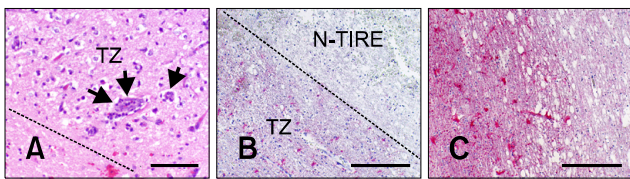


Fig. 7. N-TIRE-induced lesion transition zone (TZ). The broken gray line defines the boundary between the N-TIRE ablated region and TZ. (A) The neuropil in the TZ of Dog 2 was diffusely vacuolated and contained pervascular inflammatory cuffs (arrows; H&E). (B) An astroglial reaction in the TZ of Dog 1 (glial fibrillary acidic protein; GFAP). (C) More severe parenchymal vacuolization and astrogliosis in Dog 4 were associated with higher treatment energies (GFAP). Scale bars = 200 µm (A), 500 µm (B and C).

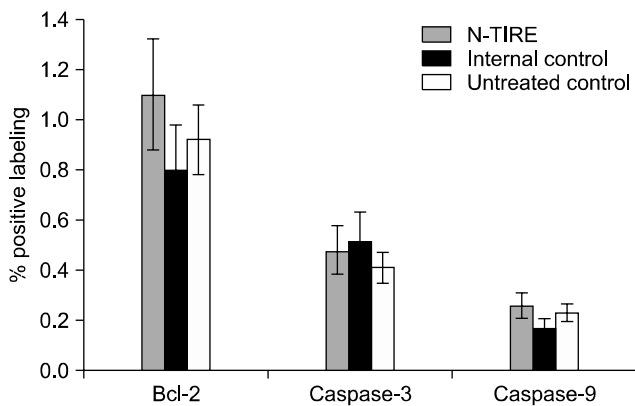


Fig. 8. Immunohistochemical evaluation of apoptosis. No differences in Bcl-2, caspase-3, and caspase-9 immunoreactivity were observed between N-TIRE-treated and control brain tissues.

We acknowledge that while our results indicate that necrosis is the predominant pathway of cell death in the N-TIRE lesions we observed, our study has several important limitations. Defining cell death with the neuropathological criteria used in this investigation lacks inherent specificity since certain morphologic criteria often attributed to necrosis such as pyknosis and karyolysis can be indicative of either apoptosis or necrosis [24]. Attempts to characterize cellular death phenotypes with singular terminology may be inappropriate since apoptosis and necrosis may represent a continuous spectrum of morphological changes modulated by common signal transduction pathways. This has led to the introduction and usage of terms such as aponecrosis. There is an increasing body of evidence suggesting that other mechanistic and morphologic forms of cell death may occur following specific types of central nervous system injury such as oncosis, aposklesis, and paratosis [24].

In our study, we examined brain tissues at only one point in time (72 h) following N-TIRE ablation. It is therefore possible that peracute histomorphologic and immunohistochemical evidence of apoptosis may have been missed. The end-point of 72 h after N-TIRE ablation was chosen because previous studies of other tissues have demonstrated that overt histomorphologic evidence of N-TIRE-induced damage may not be evident until at least 24 h following ablation [14,15,18]. In addition, the protocol we used was designed to primarily assess the neurological safety and dose-dependent relationships of applied pulse parameters by serially monitoring the clinical recovery of the dogs. This was performed after eliminating the potential effects of perioperative anesthetics and analgesics that were administered for 48 h following N-TIRE treatment. Studies of pathological changes in porcine liver and murine blood vessels performed within 12 h to 28 days post-N-TIRE have provided immunohistochemical evidence of apoptosis [14,15].

The appearance of brain edema within the TZ of N-TIRE lesions is clinically significant. Vasogenic edema formation has been observed in previous studies of N-TIRE-ablated soft tissues such as the liver [8]. This complication could have comparably dire consequences within the closed confines of the calvarium and in a sensitive tissue such as the brain. Dogs 2~4 did not experience adverse clinical effects attributable to intracranial hypertension although the N-TIRE lesions had a generally low volume and were localized in a relatively non-eloquent part of the cerebrum. Prophylactic anti-edema therapies should be considered prior to clinical application of N-TIRE in the brain, and further investigation is warranted to describe the temporal evolution of N-TIRE-associated brain edema.

Our results confirm the usefulness of imaging techniques for real-time, *in vivo* therapeutic monitoring and planning

for intracranial N-TIRE as established by other investigators using ultrasonographic imaging of the liver following N-TIRE ablation [8,14]. We previously reported on MRI and ultrasound findings indicative of N-TIRE-associated brain lesions, and visualized perilesional edema and peripheral breakdown of the blood-brain-barrier with MRI performed immediately prior to euthanasia of dogs treated with N-TIRE [9]. Gross and histopathologic examination of dogs subjected to N-TIRE provided phenotypic confirmation of the morphological changes seen with antemortem MRI. The geometry and tissue characteristics of N-TIRE-associated brain lesions on histologic preparations were analogous to their expected appearances on MRI images. N-TIRE-induced lesions were predominantly hypointense on T1W and hyperintense on T2W images (indicating brain tissue necrosis) with multifocal intralesional T2W hypointensities (suggestive of intraparenchymal hemorrhage). Peripheral capillary disruption visible within the N-TIRE-induced lesions corresponded to the contrast enhancement pattern noted during the MRI examinations. The ability to precisely monitor therapeutic outcomes in real time using standard of care techniques specific for the target organ is an essential step for demonstrating the clinical applicability of N-TIRE. It has been shown that the inherent electrical properties of complex tissues are unique due to their varying cellular structures and can change as a result of applied electroporation pulses [13,20]. Therefore, additional studies of the effects of N-TIRE on both physiologically (*i.e.*, gray vs. white matter) and pathologically (*i.e.*, malignant glioma) heterogeneous brain tissues of varying geometries are necessary before N-TIRE can be refined for clinical use.

In conclusion, we have provided histomorphologic confirmation that N-TIRE effectively and focally ablates normal brain tissue while selectively sparing the major vasculature in the treated regions. This study highlights the advantages of N-TIRE that makes this technique attractive for controlled ablation of unwanted tissue in the sensitive intracranial environment.

Acknowledgments

This work was supported in part by the Wallace Coulter and National Science Foundations (NSF-CBET 0933335). The authors thank Dr. Bernard Jortner, Dr. Elankumaran Subbiah, Ms. Jennifer Rudd, and Mrs. Barbara Wheeler for technical assistance with the ultrastructural and immunohistochemical studies. Angiodynamics, Inc. (USA) provided the NanoKnife pulse generator and electrodes used in this study.

References

1. Al-Sakere B, André F, Bernat C, Connault E, Opolon P,

- Davalos RV, Rubinsky B, Mir LM.** Tumor ablation with irreversible electroporation. *PLoS One* 2007, **2**, e1135.
2. **Atsumi H, Matsumae M, Kaneda M, Muro I, Mamata Y, Komiya T, Tsugu A, Tsugane R.** Novel laser system and laser irradiation method reduced the risk of carbonization during laser interstitial thermotherapy: assessed by MR temperature measurement. *Lasers Surg Med* 2001, **29**, 108-117.
 3. **Chen LQ, Wei JS, Lei ZN, Zhang LM, Liu Y, Sun FY.** Induction of Bcl-2 and Bax was related to hyperphosphorylation of tau and neuronal death induced by okadaic acid in rat brain. *Anat Rec A Discov Mol Cell Evol Biol* 2005, **287A**, 1236-1245.
 4. **Chizmadzhev YA, Zarnitsin VG, Weaver JC, Potts RO.** Mechanism of electroinduced ionic species transport through a multilamellar lipid system. *Biophys J* 1995, **68**, 749-765.
 5. **Cosman ER, Nashold BS, Bedenbaugh P.** Stereotactic radiofrequency lesion making. *Appl Neurophysiol* 1983, **46**, 160-166.
 6. **Davalos RV, Mir LM, Rubinsky B.** Tissue ablation with irreversible electroporation. *Ann Biomed Eng* 2005, **33**, 223-231.
 7. **Dev SB, Hofmann GA.** Electrochemotherapy-a novel method of cancer treatment. *Cancer Treat Rev* 1994, **20**, 105-115.
 8. **Edd JF, Horowitz L, Davalos RV, Mir LM, Rubinsky B.** In vivo results of a new focal tissue ablation technique: irreversible electroporation. *IEEE Trans Biomed Eng* 2006, **53**, 1409-1415.
 9. **Ellis TL, Garcia PA, Rossmeisl JH Jr., Henao-Guerrero N, Robertson J, Davalos RV.** Nonthermal irreversible electroporation for intracranial surgical applications. *J Neurosurg* 2011, **114**, 681-688.
 10. **Esiri M, Squier W, Perl D.** *Oppenheimer's Diagnostic Neuropathology: A Practical Manual*. 3rd ed. pp. 531-537, CRC Press, Boca Raton, 2006.
 11. **Foster RS, Bihrl R, Sanghvi NT, Fry FJ, Donohue JP.** High-intensity focused ultrasound in the treatment of prostatic disease. *Eur Urol* 1993, **23** (Suppl 1), 29-33.
 12. **Garcia PA, Pancotto TE, Rossmeisl JH Jr., Henao-Guerrero N, Gustafson NR, Daniel GB, Robertson JL, Ellis TL, Davalos RV.** Non-thermal irreversible electroporation (N-TIRE) and adjuvant fractionated radiotherapeutic multimodal therapy for intracranial malignant glioma in a canine patient. *Technol Cancer Res Treat* 2011, **10**, 73-83.
 13. **Garcia PA, Rossmeisl JH Jr., Neal RE II, Ellis TL, Olson JD, Henao-Guerreo N, Robertson J, Davalos RV.** Intracranial nonthermal irreversible electroporation: in vivo analysis. *J Membr Biol* 2010, **236**, 127-136.
 14. **Lee EW, Loh CT, Kee ST.** Imaging guided percutaneous irreversible electroporation: ultrasound and immunohistological correlation. *Technol Cancer Res Treat* 2007, **6**, 287-294.
 15. **Maor E, Ivorra A, Leor J, Rubinsky B.** The effect of irreversible electroporation on blood vessels. *Technol Cancer Res Treat* 2007, **6**, 307-312
 16. **Miklavčič D, Šemrov D, Mekid H, Mir LM.** A validated model of in vivo electric field distribution in tissues for electrochemotherapy and for DNA electrotransfer for gene therapy. *Biochim Biophys Acta* 2000, **1523**, 73-83.
 17. **National Research Council.** *Guide for the Care and Use of Laboratory Animals*. 8th ed. pp. 11-124, The National Academies Press, Washington, 2011.
 18. **Onik G, Mikus P, Rubinsky B.** Irreversible electroporation: implications for prostate ablation. *Technol Cancer Res Treat* 2007, **6**, 295-300.
 19. **Rubinsky B.** Irreversible electroporation in medicine. *Technol Cancer Res Treat* 2007, **6**, 255-260.
 20. **Rubinsky B, Onik G, Mikus P.** Irreversible electroporation: a new ablation modality-clinical implications. *Technol Cancer Res Treat* 2007, **6**, 37-48.
 21. **Shafiee H, Garcia PA, Davalos RV.** A preliminary study to delineate irreversible electroporation from thermal damage using the arrhenius equation. *J Biomech Eng* 2009, **131**, 074509.
 22. **Tacke J.** Thermal therapies in interventional MR imaging. Cryotherapy. *Neuroimaging Clin N Am* 2001, **11**, 759-765.
 23. **Weaver JC.** Electroporation: a general phenomenon for manipulating cells and tissues. *J Cell Biochem* 1993, **51**, 426-435.
 24. **Yakovlev AG, Faden AI.** Mechanisms of neural cell death: implications for development of neuroprotective treatment strategies. *NeuroRx* 2004, **1**, 5-16.